

CERN-EP-2023-116
21 June 2023

Observation and branching fraction measurement of the decay

$$\Xi_b^- \rightarrow \Lambda_b^0 \pi^-$$

LHCb collaboration[†]

Abstract

The decay $\Xi_b^- \rightarrow \Lambda_b^0 \pi^-$ is observed using a proton-proton collision data sample collected at center-of-mass energy $\sqrt{s} = 13$ TeV with the LHCb detector, corresponding to an integrated luminosity of 5.5 fb^{-1} . This process is mediated by the $s \rightarrow u\bar{u}d$ quark-level transition, where the b quark in the Ξ_b^- baryon is a spectator in the decay. Averaging the results obtained using the two Λ_b^0 decay modes, $\Lambda_b^0 \rightarrow \Lambda_c^+ \pi^-$ and $\Lambda_b^0 \rightarrow \Lambda_c^+ \pi^- \pi^+ \pi^-$, the relative production ratio is measured to be $(f_{\Xi_b^-}/f_{\Lambda_b^0})\mathcal{B}(\Xi_b^- \rightarrow \Lambda_b^0 \pi^-) = (7.3 \pm 0.8 \pm 0.6) \times 10^{-4}$. Here the uncertainties are statistical and systematic, respectively, and $f_{\Xi_b^-}(f_{\Lambda_b^0})$ is the fragmentation fraction for a b quark into a Ξ_b^- (Λ_b^0) baryon. Using an independent measurement of $f_{\Xi_b^-}/f_{\Lambda_b^0}$, the branching fraction $\mathcal{B}(\Xi_b^- \rightarrow \Lambda_b^0 \pi^-) = (0.89 \pm 0.10 \pm 0.07 \pm 0.29)\%$ is obtained, where the last uncertainty is due to the assumed SU(3) flavor symmetry in the determination of $f_{\Xi_b^-}/f_{\Lambda_b^0}$.

Submitted to Phys. Rev. D

© 2023 CERN for the benefit of the LHCb collaboration. CC BY 4.0 licence.

[†]Authors are listed at the end of this paper.

1 Introduction

In the constituent quark model [1, 2] quarks (antiquarks) are 3_C ($\bar{3}_C$) color-triplets (color-antitriplets) of $SU(3)_{\text{color}}$, the gauge group of Quantum Chromodynamics (QCD). Conventional mesons (baryons) are formed from the color-singlet combination of a quark and an antiquark (three quarks). More complex structures, including tetraquarks, composed of two quarks and two antiquarks, or pentaquarks, formed from four quarks and one antiquark, are expected. These states may be either compact (tightly bound), or molecular (loosely bound). Many candidates of these more exotic states have been reported over the last two decades [3, 4]. One natural way to characterize compact tetraquarks and pentaquarks is to describe them as bound states of quarks and diquarks. Diquarks are constructed from two quarks, which together form a color-antitriplet $\bar{3}_C$ of $SU(3)_{\text{color}}$. At leading order in QCD, the two quarks in a diquark exhibit an attractive force that is half as strong as that between a quark and an antiquark, when the diquark is in the $J^P = 0^+$ state. Thus compact tetraquarks may be formed from the color-singlet combination of a $\bar{3}_C$ diquark and a 3_C anti-diquark, and pentaquarks can be built from two $\bar{3}_C$ diquarks and one $\bar{3}_C$ antiquark. In this model, it is possible that some conventional baryons could be best described as the bound state of a 3_C quark with a $\bar{3}_C$ diquark. See Refs. [5, 6] for reviews on diquarks.

The weak decay $\Xi_b^- \rightarrow \Lambda_b^0 \pi^-$, where the b quark is a spectator, involves the parity-violating S -wave matrix element $sd(0^+) \rightarrow ud(0^+) + \pi^-(0^-)$ [7]. Here, the quantities in parentheses indicate the spin-parity (J^P) of the preceding quark pair or particle. There are several predictions for the size of this matrix element that lead to a branching fraction $\mathcal{B}(\Xi_b^- \rightarrow \Lambda_b^0 \pi^-)$ in the range from 0.14% to 8% [7–14]. The largest of these predictions [11, 12] is derived from a current algebra approach, and considers the possibility of enhanced short-range correlations within diquarks [15, 16] that could significantly increase the hadronic matrix element for the $\Xi_b^- \rightarrow \Lambda_b^0 \pi^-$ transition, leading to a value of $\mathcal{B}(\Xi_b^- \rightarrow \Lambda_b^0 \pi^-)$ in the range of (2–8)%. If such a large branching fraction was measured, it would be among the largest of any Ξ_b^- decay mode.

In the absence of any large enhancements to the Ξ_b^- decay rate from the sd diquark, a rough estimate of the ratio of the s quark decay rate to the b quark decay rate within the Ξ_b baryon can be obtained from the ratio of lifetimes $\tau_{\Lambda_b^0}/\tau_{\Lambda} \simeq 0.58\%$ [3]. Thus, a branching fraction for the decay $\Xi_b^- \rightarrow \Lambda_b^0 \pi^-$ anywhere in the range of (2–8)% would be rather striking, and could lend support to diquark models and enhanced short-range correlations within diquarks.

Regardless of the value for the $\Xi_b^- \rightarrow \Lambda_b^0 \pi^-$ decay rate, this contribution should be accounted for when comparing the measured Ξ_b^- lifetime to theoretical predictions, such as those made using the Heavy Quark Expansion (see Ref. [17] for a review). Such comparisons typically consider only the decay of the heavy b quark, along with higher-order corrections due to the spectator quarks, and do not include contributions from the decay of the s quark.

A previous search for the $\Xi_b^- \rightarrow \Lambda_b^0 \pi^-$ decay was performed by the LHCb collaboration using 3 fb^{-1} of proton-proton (pp) collision data at center-of-mass energies $\sqrt{s} = 7$ and 8 TeV, and found evidence for the decay at the level of 3.2σ significance [18]. This paper reports a follow-up analysis of this decay mode, and measurement of the branching fraction $\mathcal{B}(\Xi_b^- \rightarrow \Lambda_b^0 \pi^-)$. The inclusion of charge-conjugate processes is implied throughout. The measurement of $\mathcal{B}(\Xi_b^- \rightarrow \Lambda_b^0 \pi^-)$ is performed by normalizing the Ξ_b^- signal yield to the

yield of inclusively produced Λ_b^0 baryons through the equation

$$r_s \equiv \frac{f_{\Xi_b^-}}{f_{\Lambda_b^0}} \mathcal{B}(\Xi_b^- \rightarrow \Lambda_b^0 \pi^-) = \frac{N(\Xi_b^- \rightarrow \Lambda_b^0 \pi^-)}{N(\Lambda_b^0) \epsilon_{\text{rel}}}. \quad (1)$$

Here $f_{\Xi_b^-}$ and $f_{\Lambda_b^0}$ are the $b \rightarrow \Xi_b^-$ and $b \rightarrow \Lambda_b^0$ fragmentation fractions, respectively, with the ratio measured by LHCb to be $\frac{f_{\Xi_b^-}}{f_{\Lambda_b^0}} = (8.2 \pm 0.7 \pm 0.6 \pm 2.5)\%$ [19] at $\sqrt{s} = 13$ TeV.

The yield in the normalization mode, $N(\Lambda_b^0)$, is the number of selected Λ_b^0 signal decays from all sources, and $N(\Xi_b^- \rightarrow \Lambda_b^0 \pi^-)$ is the yield of $\Xi_b^- \rightarrow \Lambda_b^0 \pi^-$ signal decays. The factor $\epsilon_{\text{rel}} \equiv \epsilon_{\text{sig}}/\epsilon_{\text{norm}}$ is the relative efficiency between the signal and normalization modes.

The measurement uses pp collision data samples collected by the LHCb experiment at $\sqrt{s} = 13$ TeV, corresponding to an integrated luminosity of 5.5 fb^{-1} . The integrated luminosity and $b\bar{b}$ production cross-section are each about a factor of two larger compared to the previous analysis [18]. Moreover, the previous work used the single decay mode, $\Lambda_b^0 \rightarrow \Lambda_c^+ \pi^-$, and this analysis uses both $\Lambda_b^0 \rightarrow \Lambda_c^+ \pi^-$ and $\Lambda_b^0 \rightarrow \Lambda_c^+ \pi^- \pi^+ \pi^-$ decays. Taken together, a substantial improvement in statistical precision is expected compared to the previous measurement.

The signal for the $\Xi_b^- \rightarrow \Lambda_b^0 \pi^-$ decay is a narrow peak in the spectrum of the mass difference, $\delta M \equiv M(\Lambda_b^0 \pi^-) - M(\Lambda_b^0) - m_\pi$, where $M(\Lambda_b^0 \pi^-)$ and $M(\Lambda_b^0)$ are the reconstructed invariant masses of the respective candidates, and m_π is the known π^- mass [3]. From the known masses of the Ξ_b^- [20] and Λ_b^0 baryons [3], the peak is expected at $38.14 \pm 0.29 \text{ MeV}/c^2$.

2 Detector and simulation

The LHCb detector [21, 22] is a single-arm forward spectrometer covering the forward direction and designed for the study of particles containing b or c quarks. The detector includes a high-precision tracking system consisting of a silicon-strip vertex detector surrounding the pp interaction region [23], a large-area silicon-strip detector located upstream of a dipole magnet with a bending power of about 4 Tm, and three stations of silicon-strip detectors and straw drift tubes [24] placed downstream of the magnet. The tracking system provides a measurement of the momentum, p , of charged particles with a relative uncertainty that varies from 0.5% at low momentum to 1.0% at 200 GeV/ c . The minimum distance of a track to a primary pp collision vertex (PV), the impact parameter (IP), is measured with a resolution of $\sigma_{\text{IP}} = (15 + 29/p_{\text{T}}) \mu\text{m}$, where p_{T} is the component of the momentum transverse to the beam, in GeV/ c . Different types of charged hadrons are distinguished using information from two ring-imaging Cherenkov detectors [25]. Photons, electrons and hadrons are identified by a calorimeter system consisting of scintillating-pad and preshower detectors, an electromagnetic and a hadronic calorimeter. Muons are identified by a system composed of alternating layers of iron and multiwire proportional chambers [26]. The online event selection is performed by a trigger [27], which consists of a hardware stage, based on information from the calorimeter and muon systems, followed by a software stage, which applies a full event reconstruction. The software stage employs a multivariate algorithm [28, 29] to identify secondary vertices consistent with the decay of a b hadron.

Simulation is required to model the effects of the detector acceptance and the imposed selection requirements. In the simulation, pp collisions are generated using PYTHIA [30] with a specific LHCb configuration [31]. Decays of unstable particles are described by EVTGEN [32], in which final-state radiation is generated using PHOTOS [33]. The interaction of the generated particles with the detector, and its response, are implemented using the GEANT4 toolkit [34] as described in Ref. [35]. The underlying pp interaction is reused multiple times, with an independently generated signal decay for each one [36].

3 Event selection

Two samples of Λ_b^0 candidates are reconstructed, one composed of $\Lambda_c^+ \rightarrow pK^-\pi^+$ candidates combined with a single π^- (1π sample), and a second formed by pairing Λ_c^+ candidates with three pions, $\pi^-\pi^+\pi^-$ (3π sample). All final-state tracks are required to be significantly detached from all PVs in the event, pass loose particle identification (PID) criteria for the particle to be consistent with the assumed decay, and have $p_T > 100$ MeV/ c . The Λ_c^+ baryon is required to have $|M(pK^-\pi^+) - m_{\Lambda_c^+}| < 25$ MeV/ c^2 , where $m_{\Lambda_c^+}$ is the known Λ_c^+ mass [3], and have a decay time in the range $-0.5 < t < 5$ ps. For the latter, the negative lower bound allows for finite resolution of the Λ_c^+ baryon decay time. For the $\Lambda_b^0 \rightarrow \Lambda_c^+\pi^-\pi^+\pi^-$ decay, the dominant resonant feature of the $\pi^-\pi^+\pi^-$ system is the contribution from the broad $a_1(1260)^-$ resonance. Since the combinatorial background under the Λ_b^0 baryon signal peak rises steeply with $M(\pi^-\pi^+\pi^-)$, a requirement of $M(\pi^-\pi^+\pi^-) < 2800$ MeV/ c^2 is imposed, which retains about 90% of the signal. Each Λ_b^0 candidate is assigned to the PV for which χ_{IP}^2 is smallest, where χ_{IP}^2 is the increase in χ^2 of the PV fit when the particle under consideration is included in the fit. To a good approximation, $\chi_{\text{IP}}^2 \simeq (\text{IP}/\sigma_{\text{IP}})^2$, and all decay products of the Λ_b^0 candidate are required to have $\chi_{\text{IP}}^2 > 4$.

Backgrounds from other b -hadron decays, where the Λ_c^+ candidate is compatible with a misidentified D meson, are suppressed by re-computing the three-body mass with the $D^+ \rightarrow K^-\pi^+\pi^+$, $K^+K^-\pi^+$, $D_s^+ \rightarrow K^+K^-\pi^+$, $D^{*+} \rightarrow (D^0 \rightarrow K^+K^-)\pi^+$ mass hypotheses, and applying stringent PID requirements if the mass is consistent with any of the above charm mesons within about twice its resolution. A similar procedure is employed to remove the contribution from $\phi \rightarrow K^+K^-$ decays where the K^+ is misidentified as a proton. The efficiency of this veto is about 98% on simulated signal decays, while removing about 15% of the misidentified backgrounds.

In a small fraction of cases, a single particle in the vertex detector can be misreconstructed as two distinct tracks that have almost zero opening angle. This background is removed by requiring all pairs of final-state tracks in the decay to have an opening angle larger than 0.8 mrad. The efficiency of this requirement on simulated Λ_b^0 decays is 99.8%, while suppressing the mis-reconstruction background by 3% (14%) for the $\Lambda_b^0 \rightarrow \Lambda_c^+\pi^-$ ($\Lambda_b^0 \rightarrow \Lambda_c^+\pi^-\pi^+\pi^-$) candidates.

The Ξ_b^- sample is formed by combining each Λ_b^0 candidate satisfying $5560 < M(\Lambda_b^0) < 5680$ MeV/ c^2 with a π^- meson candidate. The π^- meson must pass loose PID requirements, have $p_T > 100$ MeV/ c , and have an opening angle larger than 0.8 mrad relative to each of the other final-state particles of the Ξ_b^- candidate. No requirement is imposed on χ_{IP}^2 for the π^- meson, because its low p_T , about 0.35 GeV/ c on average for those pions that are reconstructed, leads to a relatively large uncertainty on σ_{IP} . The fitted Ξ_b^- decay vertex is required to have good fit quality. Using the same

selection criteria as the right-sign (RS) $\Lambda_b^0\pi^-$ combinations, wrong-sign (WS) combinations are also formed to study the combinatorial background, and to train the multivariate discriminants discussed below. When there are multiple candidates in an event, which happens in a few percent of selected events, all candidates are retained. The Λ_b^0 and Ξ_b^- baryons are required to be within the fiducial region $p_T < 20 \text{ GeV}/c$ and $2 < \eta < 6$, which is the region in which $f_{\Xi_b^-}/f_{\Lambda_b^0}$ was measured [19].

To improve the signal-to-background ratio in the Λ_b^0 normalization and Ξ_b^- signal modes, two pairs of boosted decision tree (BDT) classifiers [37–39] with gradient boosting are employed. The first pair (BDT1), one applied to the 1π and the second for the 3π mode, is used to suppress the combinatorial background under the Λ_b^0 signal peak. The second pair (BDT2) suppresses the combinatorial background under the Ξ_b^- signal peak. Each classifier has an output variable that ranges from -1 to 1 , with the signal (background) events peaking toward 1 (-1).

The optimization of these BDT algorithms requires accurate determination of the efficiency from simulation. Two weights are applied to the simulated events to account for the differences in the kinematical distributions in the final state between data and simulation. The first weight accounts for the differences in the (p_T, η) production spectra of the beauty baryons. For the Λ_b^0 decays, the weights are obtained from the ratio of the background-subtracted (p_T, η) distributions in $\Lambda_b^0 \rightarrow \Lambda_c^+\pi^-(\pi^+\pi^-)$ data using the *sPlot* method [40] and simulated signal decays. For the Ξ_b^- simulation, (p_T, η) weights are obtained from the $\Xi_b^- \rightarrow \Xi_c^0\pi^-$ decay, where $\Xi_c^0 \rightarrow pK^-K^-\pi^+$.

The second weight accounts for imperfect modeling of the resonant contributions to the $\Lambda_c^+ \rightarrow pK^-\pi^+$ decay. This weight is a function of the pair of invariant masses $[m(pK^-), m(K^-\pi^+)]$ in the Λ_c^+ decay, and are obtained from large samples of semileptonic $\Lambda_b^0 \rightarrow \Lambda_c^+\mu\nu_\mu X$ decays in data and simulation. Both weights are applied when computing all efficiencies.

The BDT1 classifiers use a combination of geometric, kinematic and PID variables to distinguish signal from background. The geometric quantities include the χ_{IP}^2 of all final-state particles, the three-dimensional and radial flight distances of the Λ_b^0 candidate decay vertex from its associated PV, the χ^2 of the Λ_b^0 candidate vertex fit, the angle $\theta_{\vec{p}, V}$ between the momentum vector of the Λ_b^0 candidate and the line that joins the Λ_b^0 decay vertex and the PV, the χ^2 of the Λ_c^+ decay-vertex fit, and the decay time of the Λ_c^+ candidate. The kinematical quantities include the total momentum and transverse momentum of each final-state particle. For each particle, a probability for the assigned PID hypothesis [41] is also used. The PID response of the charged hadrons in the simulated signal and normalization mode decays is obtained from dedicated calibration samples from the data where no PID requirements are imposed [25, 41]. For the 3π sample, two additional variables, $M(\pi^-\pi^+\pi^-)$ and the χ^2 of the vertex separation between the 3π vertex and the PV, are included.

To train the BDT1 classifiers, signal Λ_b^0 decays are taken from simulated $\Xi_b^- \rightarrow \Lambda_b^0\pi^-$ decays, where the Λ_b^0 baryon is forced to decay into either the $\Lambda_c^+\pi^-$ or $\Lambda_c^+\pi^-\pi^+\pi^-$ mode. The latter is simulated with a number of intermediate resonances to reproduce the two and three-body masses observed in the data. The usage of the $\Xi_b^- \rightarrow \Lambda_b^0\pi^-$ simulation will favor selecting Λ_b^0 baryons that are produced in the decay of a Ξ_b^- baryon. The combinatorial background sample for the BDT1 training is composed of Λ_b^0 candidates in the data that have invariant mass in the range $5700 < M(\Lambda_c^+\pi^-[\pi^+\pi^-]) < 5850 \text{ MeV}/c^2$.

The optimal requirement on the BDT1 response for each Λ_b^0 decay mode is determined

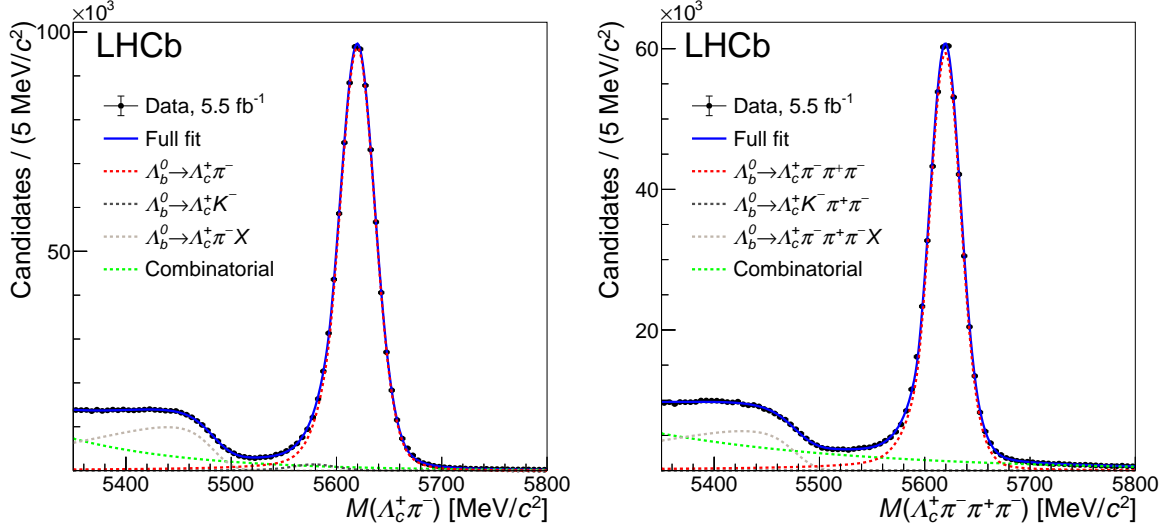


Figure 1: Invariant-mass spectra of (left) $\Lambda_b^0 \rightarrow \Lambda_c^+ \pi^-$ and (right) $\Lambda_b^0 \rightarrow \Lambda_c^+ \pi^- \pi^+ \pi^-$ candidates for the full data sample. The fitted signal and background shapes, as described in the text, are overlaid.

by taking the maximum value of the figure of merit (FOM), defined as $\text{FOM} = S/\sqrt{S+B}$, where $S = S_0 \epsilon_{\text{BDT1}}$. The estimated number of Ξ_b^- signal decays with no BDT1 requirement, S_0 , is taken to be 200, based on an extrapolation of the results in Ref. [18], and ϵ_{BDT1} is the efficiency of the BDT1 requirement on simulated signal decays, which includes the weights discussed previously. The quantity B is the expected number of background events in the range $34.8 < \delta M < 41.6 \text{ MeV}/c^2$, about 2.5 times the expected mass resolution. The FOM is found to have a broad and nearly flat maximum with a drop near the endpoints of -1 and 1 . A loose requirement of $\text{BDT1} > 0$ is chosen for both Λ_b^0 modes, resulting in an efficiency of 93% for selecting Λ_b^0 baryons in $\Xi_b^- \rightarrow \Lambda_b^0 \pi^-$ decays and 87% for promptly produced Λ_b^0 baryons, while removing about 80% of the combinatorial background.

The mass spectra of Λ_b^0 candidates passing all selection requirements, except the final Λ_b^0 mass window of $5560 < M(\Lambda_b^0) < 5680 \text{ MeV}/c^2$, are shown in Fig. 1. The mass distributions are described as the sum of a signal shape and several background components, and a binned extended maximum-likelihood fit is performed to obtain the Λ_b^0 signal yields. The signal shapes are obtained from simulated decays, and are modeled as the sum of two Crystal Ball functions [42] with power law tails on each side and a common peak value. All parameters are fixed to the values estimated from the simulation except for the peak mass value and an overall scale factor for the resolution to account for a small difference between the mass resolution in data and simulation. The invariant mass shapes describing the partially reconstructed $\Lambda_b^0 \rightarrow \Lambda_c^+ \pi^- (\pi^+ \pi^-) X$ decays, where X represents one or more missing particles, and misidentified $\Lambda_b^0 \rightarrow \Lambda_c^+ K^- (\pi^+ \pi^-)$ background contributions are based on simulated decays, and are described in Ref. [43]. The combinatorial background is parameterized with an exponential function. Signal yields of $(921 \pm 1) \times 10^3$ and $(511 \pm 1) \times 10^3$ in the full fit range are obtained in the $\Lambda_b^0 \rightarrow \Lambda_c^+ \pi^-$ and $\Lambda_b^0 \rightarrow \Lambda_c^+ \pi^- \pi^+ \pi^-$ modes, respectively. The mass resolution scale factor is 1.1, which is consistent with that found in other b -hadron decay analyses. The background-to-signal ratios in the signal region from 5560–5680 MeV/c^2 are 2.1% and 6.8% for the $\Lambda_b^0 \rightarrow \Lambda_c^+ \pi^-$ and $\Lambda_b^0 \rightarrow \Lambda_c^+ \pi^- \pi^+ \pi^-$

Table 1: Efficiencies for the two BDT2 selections on simulated Ξ_b^- signal decays and on WS background (in %) for the two Λ_b^0 final states. The FOM values are also shown. Uncertainties are statistical only.

BDT2 selection	$\epsilon_{\text{BDT2}}^{\Xi_b^-}$		$\epsilon_{\text{BDT2}}^{\text{bkg}}$		FOM	
	$\Lambda_c^+\pi^-$	$\Lambda_c^+\pi^-\pi^+\pi^-$	$\Lambda_c^+\pi^-$	$\Lambda_c^+\pi^-\pi^+\pi^-$	$\Lambda_c^+\pi^-$	$\Lambda_c^+\pi^-\pi^+\pi^-$
Tight	35.6 ± 0.2	39.9 ± 0.2	0.6 ± 0.1	1.1 ± 0.1	5.4	6.2
Loose	46.1 ± 0.2	51.8 ± 0.2	1.4 ± 0.1	2.6 ± 0.2	5.0	5.7

decay modes, respectively.

In forming the Ξ_b^- candidates, the major sources of background are from random combinations of Λ_b^0 baryons and π^- mesons, and from the strong decays $\Sigma_b^{(*)-} \rightarrow \Lambda_b^0\pi^-$. Both of these backgrounds have a candidate decay-time distribution that peaks at zero, whereas the signal has preferentially positive decay times. Ordinarily, this would be a powerful discriminant against background, but due to the low π^- meson momentum and relatively small opening angle in the Ξ_b^- baryon decay, the uncertainty on the Ξ_b^- vertex position is large. The resolution on the z coordinate of the Ξ_b^- decay vertex is about 7 mm, which is to be compared to about 0.5 mm for the Λ_b^0 decay vertex. This relatively large uncertainty makes it more challenging to separate $\Lambda_b^0\pi^-$ background from the $\Xi_b^- \rightarrow \Lambda_b^0\pi^-$ signal.

The second BDT classifier, BDT2, is employed to suppress combinatorial background, primarily from prompt $\Lambda_b^0\pi^-$ combinations, and uses 12 discriminating variables: the p_T , flight distance, and $\theta_{\bar{p},V}$ of the Ξ_b^- candidate; the decay time, p and p_T of the Λ_b^0 baryon; the p , p_T and χ_{IP}^2 of the π^- meson and its associated PID probability to be a pion; and $\eta(\Lambda_b^0) - \eta(\pi^-)$ and $\phi(\Lambda_b^0) - \phi(\pi^-)$, where $\eta(X)$ and $\phi(X)$ are the pseudorapidity and azimuthal angle of the indicated particles. Simulated signal decays are used to train the BDT2 classifier. Wrong-sign candidates within 2.5σ of the expected signal peak position in δM are used to represent the background.

A second FOM, defined in an analogous way to that of BDT1, is used to optimize the BDT2 selection requirement. The maximum value of the FOM corresponds to BDT2 > 0.9, which is used for the signal significance. For the branching fraction measurement, a looser requirement of BDT2 > 0.8 is used, which gives about 30% higher relative efficiency according to simulation with only a slightly lower FOM. Hereafter, these are referred to as the tight (BDT2 > 0.9) and loose (BDT2 > 0.8) selections. The looser selection on BDT2 reduces the systematic uncertainty associated with the BDT2 requirement. The two BDT2 requirements, their efficiencies and FOM values are shown in Table 1.

Figure 2 shows the δM spectra for the selected $\Xi_b^- \rightarrow \Lambda_b^0\pi^-$ signal candidates passing the tight BDT2 requirement for the $\Lambda_b^0 \rightarrow \Lambda_c^+\pi^-$ and $\Lambda_b^0 \rightarrow \Lambda_c^+\pi^-\pi^+\pi^-$ samples. The corresponding distributions with the loose BDT2 selection for the r_s measurement are shown in Fig. 3. In both cases, there are clear peaks at the expected location for a Ξ_b^- signal in the RS spectra, and no such peak in the WS spectra.

A simultaneous unbinned extended maximum likelihood fit to the four (RS and WS for each Λ_b^0 mode) δM spectra is performed to obtain the Ξ_b^- signal yields. The spectra

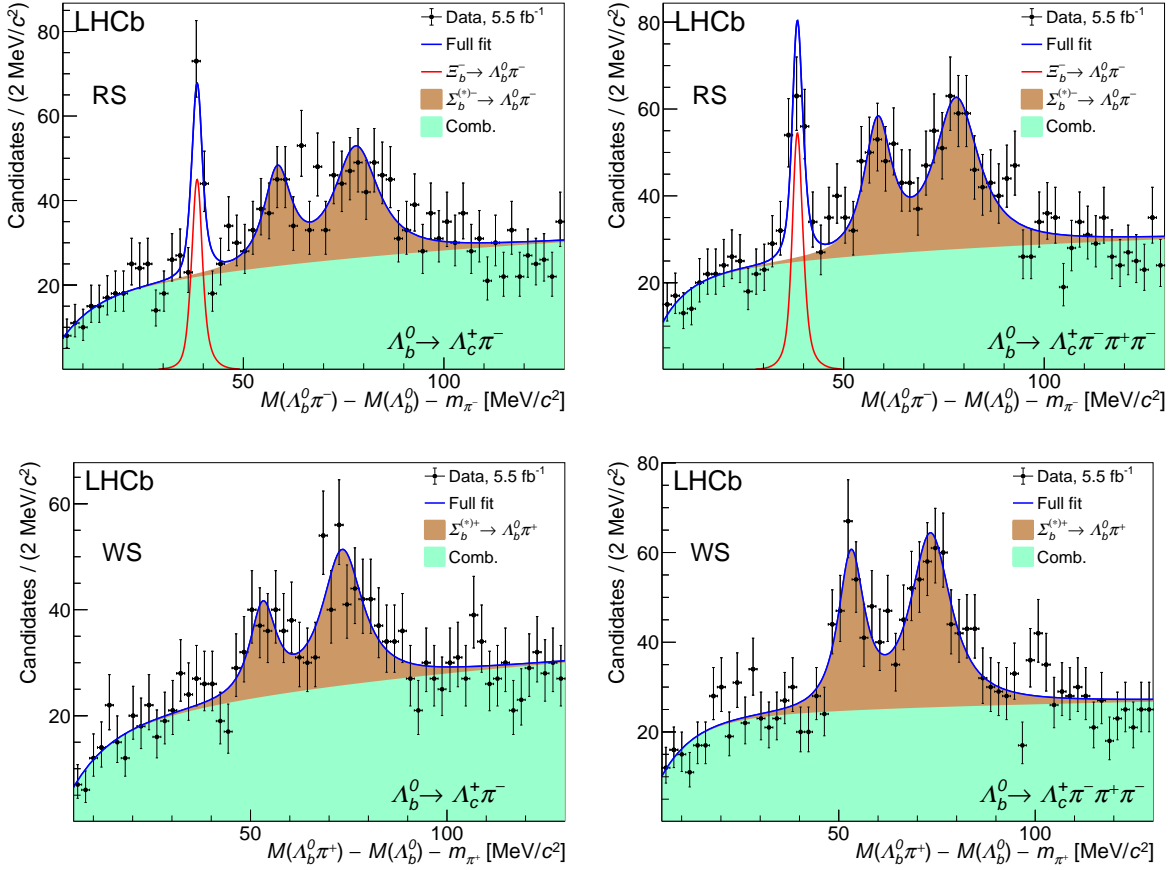


Figure 2: (Top row) Spectra of the mass difference, $M(\Lambda_b^0\pi^-) - M(\Lambda_b^0) - m_{\pi^-}$ for $\Xi_b^- \rightarrow \Lambda_b^0\pi^-$ candidates, for the (left) $\Lambda_b^0 \rightarrow \Lambda_c^+\pi^-$ and (right) $\Lambda_b^0 \rightarrow \Lambda_c^+\pi^-\pi^+\pi^-$ right-sign samples, with the tight BDT2 selection. The bottom row shows the corresponding distributions for the wrong-sign candidates. Fits to the data are overlaid as described in the text.

are modeled as the sum of a Ξ_b^- signal shape, and background shapes for the $\Sigma_b^{(*)\pm}$ resonances and random $\Lambda_b^0\pi^-$ combinations. The Ξ_b^- signal shape for each Λ_b^0 mode are obtained from simulated signal decays, and is described by the sum of two Crystal Ball functions [42]. All shape parameters are fixed to the values obtained from simulation except for the peak mass value. When fitting the data, the mass resolution parameters in the Crystal Ball function are scaled by 1.1 to account for the larger mass resolution in data than in simulation. The $\Sigma_b^{(*)\pm}$ resonances are modeled by a relativistic Breit–Wigner function, as described in Ref. [18], convolved with the mass resolution. The peak mass values of the $\Sigma_b^{(*)\pm}$ signals are biased by about $+2\text{ MeV}/c^2$ due to the selection favoring those decays that are reconstructed with positive displacement relative to the PV, and for this reason, the peak mass values are allowed to vary freely in the fit. The widths are fixed to the world average values [3]. The combinatorial background is described by a threshold function of the form $(\delta M)^A(1 - e^{-\delta M/C})$. The parameters A and C are freely varied in the loose BDT fit, but the low background level in the tight BDT fit is insufficient to constrain the parameter A . It is therefore fixed in the tight BDT fit to the value obtained in the loose BDT fit. Among the freely varied parameters in the fit, only the peak mass values of the Ξ_b^- signal and the $\Sigma_b^{(*)\pm}$ resonances are shared between the two Λ_b^0 modes.

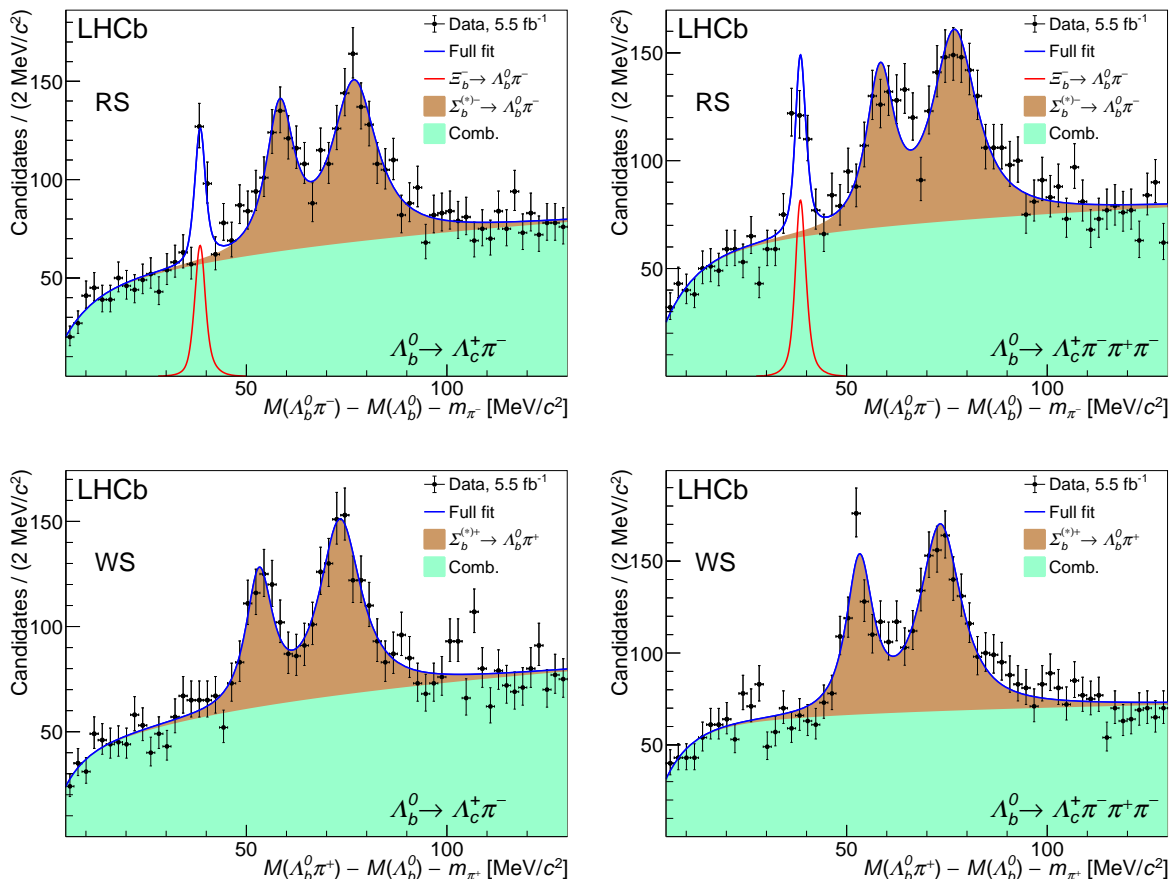


Figure 3: (Top row) Spectra of the mass difference, $M(\Lambda_b^0 \pi^-) - M(\Lambda_b^0) - m_{\pi^-}$ for $\Xi_b^- \rightarrow \Lambda_b^0 \pi^-$ candidates, for the (left) $\Lambda_b^0 \rightarrow \Lambda_c^+ \pi^-$ and (right) $\Lambda_b^0 \rightarrow \Lambda_c^+ \pi^- \pi^+ \pi^-$ right-sign samples with the loose BDT2 selection. The bottom row shows the corresponding distributions for the wrong-sign candidates. Fits to the data are overlaid as described in the text.

The results of the fits are overlaid in Figs 2 and 3. The Ξ_b^- signal yields with the tight BDT2 selection, used only for maximizing the signal significance, are 85 ± 13 and 103 ± 15 for the $\Lambda_b^0 \rightarrow \Lambda_c^+ \pi^-$ and $\Lambda_b^0 \rightarrow \Lambda_c^+ \pi^- \pi^+ \pi^-$ modes, respectively. Using Wilks theorem [44], the significance of the pair of Ξ_b^- signal peaks corresponds to about 11σ , thus definitively establishing the first observation of the $\Xi_b^- \rightarrow \Lambda_b^0 \pi^-$ decay. For the loose BDT2 selection, the corresponding Ξ_b^- signal yields are 126 ± 19 and 154 ± 23 . The larger yield in the 3π mode is anticipated, based upon the larger relative efficiency (discussed later) and the measured yields of Λ_b^0 decays. The Ξ_b^- peak position in δM is at 38.5 ± 0.2 (stat) MeV/c^2 , which is about 1σ from the value of $38.14 \pm 0.29 \text{ MeV}/c^2$, based on a recent precise measurement of the Ξ_b^- mass using $\Xi_b^- \rightarrow \Xi_c^0 \pi^-$ decays [20]. No narrow peaks are seen in the WS spectra. Corresponding fits to the combined sample, where the fraction of Ξ_b^- signal in the $\Lambda_b^0 \rightarrow \Lambda_c^+ \pi^-$ mode is fixed to 45% of the total, are shown in Fig. 4.

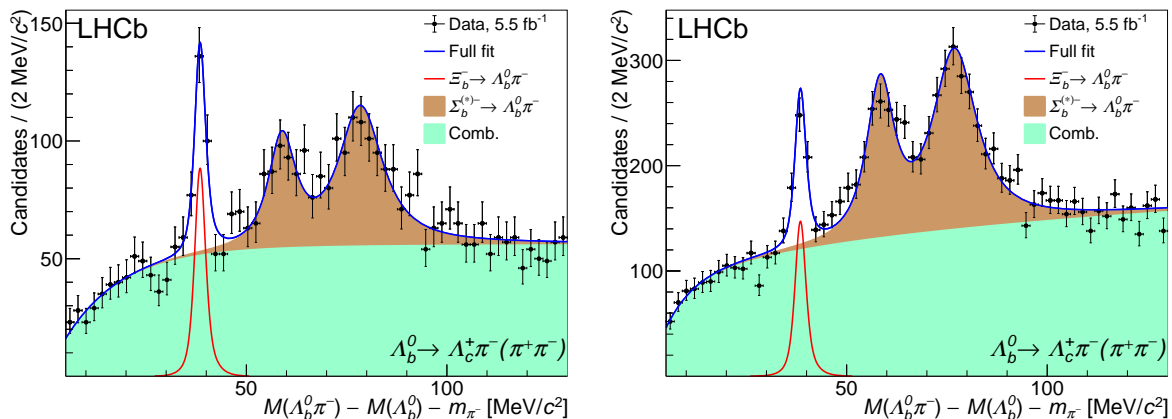


Figure 4: Spectra of the mass difference, $M(\Lambda_b^0 \pi^-) - M(\Lambda_b^0) - m_{\pi^-}$ for $\Xi_b^- \rightarrow \Lambda_b^0 \pi^-$ candidates for the combined $\Lambda_b^0 \rightarrow \Lambda_c^+ \pi^-$ and $\Lambda_b^0 \rightarrow \Lambda_c^+ \pi^- \pi^+ \pi^-$ samples for (left) tight BDT2 selection and (right) loose BDT2 selection.

4 Selection efficiencies

Simulated decays of the signal and normalization modes are used to estimate the relative efficiency, $\epsilon_{\text{rel}} = \epsilon_{\text{sig}}/\epsilon_{\text{norm}}$, where ϵ_{sig} (ϵ_{norm}) refers to the efficiency to reconstruct and select the Ξ_b^- signal (Λ_b^0 normalization) mode. For the normalization mode efficiency, production of Λ_b^0 baryons through weak decays, which contribute at the 10^{-3} level, are neglected. Relative efficiencies are determined for each of the Λ_b^0 decay modes, $\Lambda_c^+ \pi^-$ and $\Lambda_c^+ \pi^- \pi^+ \pi^-$. The relative efficiencies are computed within the $p_T < 20 \text{ GeV}/c$, $2 < \eta < 6$ fiducial acceptance. Since the Λ_b^0 decay is common to the signal and normalization mode, and the low momentum pion from the Ξ_b^- decay contributes negligibly to the hardware or software trigger, no specific selections are made on the trigger decisions.

To account for small differences between the simulation and data, a multiplicative correction to the relative efficiency is applied, defined as

$$\epsilon_{\text{rel}}^{\text{corr}} = \epsilon_{\text{rel}}^{\text{track}} \epsilon_{\text{rel}}^{\text{BDT2}} \epsilon_{\text{rel}}^{\text{trig}}. \quad (2)$$

The first correction accounts for small differences in the tracking efficiency, and is measured using large samples of $J/\psi \rightarrow \mu^+ \mu^-$ calibration samples [45]. A correction factor $\epsilon_{\text{rel}}^{\text{track}} = 0.99 \pm 0.03$ is obtained.

The source of the second correction is the BDT2 requirement. The simulation indicates an efficiency of about 50% for the loose BDT2 selection. To probe whether the BDT2 distribution in data and simulation are compatible, the signal yield ratio, r_{BDT2} , for the loose to tight BDT2 selection is compared. From the fitted yields in the two cases, the ratios are $r_{\text{BDT2}}^{1\pi} = 1.48 \pm 0.17$ and $r_{\text{BDT2}}^{3\pi} = 1.50 \pm 0.18$, where the expected value using efficiencies from simulation is 1.30 for both Λ_b^0 decay modes. Although both ratios in data are within about one standard deviation of the expected value, they are both larger, suggesting that the BDT2 response from simulation may be more strongly peaked at unity than the data. This supposition is supported by comparing the BDT1 distributions in simulation and background-subtracted data, where the large Λ_b^0 sample in simulation is seen to be more sharply peaked at unity than the data. A correction is derived by smearing the BDT2 distribution from simulation with a one-sided Gaussian function in

order to reproduce the r_{BDT2} values obtained in data. The values of $\epsilon_{\text{rel}}^{\text{BDT2}}$ obtained are 0.94 ± 0.03 and 0.93 ± 0.04 for the 1π and 3π modes, respectively.

The third correction accounts for a slightly different hardware trigger efficiency between data and simulation. Two classes of events are studied: (1) those events where the signal decay products result in the event passing the hardware trigger (TOS, short for Triggered on Signal), and (2) cases where other activity in the event, such as the other b hadron or the beam fragments, produces the hardware trigger (TIS, short for Triggered Independently of the Signal). Both are studied in data and simulation using the TISTOS method [46]. A given event can pass the TOS, TIS, or both the TOS and TIS requirements. Briefly, by selecting TIS events, one can measure the efficiency of TOS events, and vice versa. The benefit of this method is that it can be applied identically to both data and simulation. Using this method, the relative trigger efficiency between data and simulation, $\epsilon_{\text{rel}}^{\text{trig}}$, is found to be 1.033 ± 0.017 and 1.008 ± 0.004 for the 1π and 3π samples, respectively.

The products of the three correction factors, $\epsilon_{\text{rel}}^{\text{corr}}$, are 0.972 ± 0.046 and 0.941 ± 0.046 for the $\Lambda_b^0 \rightarrow \Lambda_c^+ \pi^-$ and $\Lambda_b^0 \rightarrow \Lambda_c^+ \pi^- \pi^+ \pi^-$ decay modes, respectively. For the loose BDT2 requirement, the relative efficiencies, including the above corrections, are found to be

$$\epsilon_{\text{rel}}^{\Lambda_c^+ \pi^-} = 0.210 \pm 0.004 \text{ (stat)}, \quad (3)$$

$$\epsilon_{\text{rel}}^{\Lambda_c^+ \pi^- \pi^+ \pi^-} = 0.394 \pm 0.008 \text{ (stat)}. \quad (4)$$

A significantly larger relative efficiency is obtained when the Ξ_b^- signal decay is reconstructed in the $\Lambda_b^0 \rightarrow \Lambda_c^+ \pi^- \pi^+ \pi^-$ mode as compared to the $\Lambda_c^+ \pi^-$ mode. There are two main factors that contribute to this enhancement. The first arises from the χ_{IP}^2 -related selection requirements in the trigger and analysis-related selections. In the $\Lambda_c^+ \pi^-$ mode, all final-state particles tend to have fairly high p_{T} , and thus large values of χ_{IP}^2 . The larger decay distance of the Λ_b^0 baryon from the PV in the signal mode leads to only moderate increases in ϵ_{sig} relative to ϵ_{norm} . However, for the $\Lambda_c^+ \pi^- \pi^+ \pi^-$ final state, the 3 pions tend to have lower p_{T} , leading to smaller values of χ_{IP}^2 . If any of the pions have $\chi_{\text{IP}}^2 < 4$, the Λ_b^0 candidate is not selected. The combination of (1) the larger displacement of the Λ_b^0 baryon from the PV (due to the Ξ_b^- baryon lifetime) for the signal mode as compared to the normalization mode and (2) the lower p_{T} of the pions, leads to a significantly larger increase in ϵ_{sig} relative to ϵ_{norm} for the $\Lambda_c^+ \pi^- \pi^+ \pi^-$ final state. The second effect that contributes to the increase in ϵ_{rel} is the difference in the average p and p_{T} of reconstructed Λ_b^0 decays for each of the two final states. Higher multiplicity final states must, on average, have larger momentum in order to be reconstructed and pass all selection requirements. This requires a higher momentum Ξ_b^- baryon when reconstructed in the 3π mode than the 1π mode, which in turn leads to a higher relative efficiency for reconstructing the π^- from the Ξ_b^- decay.

A summary of the yields in the signal and normalization modes, the relative efficiencies, and the computed r_s values are shown in Table 2. The Λ_b^0 yields include about a 1% contribution from misidentified $\Lambda_b^0 \rightarrow \Lambda_c^+ K^- (\pi^+ \pi^-)$ decays, which also have a narrow peak in δM at about $38 \text{ MeV}/c^2$. The r_s values for the two Λ_b^0 modes are statistically compatible with each other.

Table 2: Summary of the yields in the signal ($N(\Xi_b^-)$) and normalization modes ($N(\Lambda_b^0)$), the relative efficiencies (ϵ_{rel}), and the resulting r_s values for the loose BDT selection. The Λ_b^0 signal yields are in the invariant-mass region $5560 < M(\Lambda_b^0) < 5680 \text{ MeV}/c^2$. Uncertainties are statistical only.

Fit parameter	$\Lambda_c^+ \pi^-$	$\Lambda_c^+ \pi^- \pi^+ \pi^-$
$N(\Xi_b^- \rightarrow \Lambda_b^0 \pi^-)$	126 ± 19	154 ± 23
$N(\Lambda_b^0) [10^3]$	879 ± 1	483 ± 1
$\epsilon_{\text{rel}} [10^{-2}]$	21.0 ± 0.4	39.4 ± 0.8
$r_s [10^{-4}]$	6.80 ± 1.05	8.09 ± 1.23

Table 3: Systematic uncertainties in the measurement of r_s for each of the two decay modes of the Λ_b^0 baryon. The horizontal dividing line separates the uncorrelated (above) and correlated (below) uncertainties. For the latter, the listed sources are 100% correlated between the two Λ_b^0 decay modes.

Source	Value (%)	
	$\Lambda_c^+ \pi^-$	$\Lambda_c^+ \pi^- \pi^+ \pi^-$
Ξ_b^- signal shape	1.4	2.4
Ξ_b^- background shape	3.1	1.8
Λ_b^0 signal shape	0.3	0.8
Λ_b^0 background shape	0.1	0.7
Geom. acceptance	1.8	1.8
Sim. weights & sample sizes	3.6	3.4
Trigger efficiency	1.7	0.4
Ξ_b^- p_T spectrum	3.2	5.6
IP resolution	1.3	0.7
BDT2 efficiency	3.0	3.5
Tracking efficiency	3.3	3.3
Multiple candidates	0.5	2.6
Ξ_b^- lifetime	3.0	2.5
Total	8.5	9.7

5 Systematic uncertainties

Systematic uncertainties on r_s are summarized in Table 3, and have contributions related to the determination of the signal and normalization mode yields and the relative efficiencies. The systematic uncertainty in the Ξ_b^- signal yields is obtained from the fractional difference in the yields when increasing and decreasing the resolution scale factor by $\pm 5\%$. For the normalization modes, different bin widths and fits allowing all Λ_b^0 shape parameters to vary freely are performed. The bin widths have negligible effect on the signal yields. The change in the Λ_b^0 yield between the alternative and baseline fit is assigned as the systematic uncertainty. The Λ_b^0 background shape uncertainty is taken as the fractional change in yield when using a second-order Chebychev polynomial in place of the baseline shape. For the

Ξ_b^- combinatorial background, the fractional change in yield between the baseline shape and the alternative three-parameter function $\mathcal{P}(\delta M) = f(1 - e^{-\delta M/A}) + (1 - f)(1 - e^{-\delta M/B})$ is assigned as the systematic uncertainty.

For the relative efficiency, a number of systematic uncertainties are considered. Those uncertainties associated with the selections on the Λ_b^0 candidates are common to both the signal and normalization mode, and are significantly reduced.

The uncertainty in the geometric acceptance is due to the usage of finite-sized samples of simulated decays. The weights applied to the simulated decays to replicate the (p_T, η) distributions in data are limited by the finite yields of $\Lambda_b^0 \rightarrow \Lambda_c^+ \pi^- (\pi^+ \pi^-)$ and $\Xi_b^- \rightarrow \Xi_c^0 \pi^-$ decays in simulation and in the data. The uncertainty is assigned by varying all of the weights within their uncertainties, and recomputing the relative efficiency. This procedure is carried out 100 times, and the standard deviation of the ϵ_{rel} distribution is assigned as the uncertainty.

The Ξ_b^- efficiencies are obtained from simulated signal decays, where the signal weights are obtained from $\Xi_b^- \rightarrow \Xi^0 \pi^-$ decays. Because of differing kinematics between the control and $\Xi_b^- \rightarrow \Lambda_b^0 \pi^-$ modes, the assigned weights could have some small biases. To estimate the potential magnitude of this bias, the relative efficiencies are re-evaluated using the Λ_b^0 weights for the signal mode in place of the Ξ_b^- weights. The fractional change in the relative efficiency is assigned as the systematic uncertainty.

The IP resolution shows some small differences between data and simulation. To estimate how the difference impacts the relative efficiency, a scaling of the $\log(\chi_{\text{IP}}^2)$ values of each track is performed that brings the χ_{IP}^2 distributions in data and simulation into good agreement. With the scaling, some of the final-state tracks will fail the $\chi_{\text{IP}}^2 > 4$ requirement, leading to a reduction in the selection efficiency. The procedure is applied to both the signal and normalization modes, and the fractional change in the relative efficiency is assigned as the systematic uncertainty.

As discussed previously, the BDT2 distribution in simulation is smeared to obtain an efficiency correction for the loose BDT2 requirement, and the uncertainty is taken to be 50% of the difference of the correction factor from unity. Similarly, the uncertainty in the relative trigger efficiency is assigned to be half of the applied correction.

The tracking efficiency is calibrated using large samples of $J/\psi \rightarrow \mu^+ \mu^-$ decays, and provide a data-to-simulation correction for tracks in the momentum range from 5–200 GeV/c and $1.9 < \eta < 4.9$ [45]. The corrections are mostly within (1–2)% of unity. About 65% of the π^- mesons from the Ξ_b^- decay have momentum below 5 GeV/c, and for these cases, the correction at 5 GeV/c is used with an uncertainty that is inflated by a factor of two. The luminosity-weighted average correction is 0.99 ± 0.03 . An additional 1.4% uncertainty is assigned due to a potential difference in the number of hadronic interaction lengths in the simulated and actual detector.

A possible bias due to keeping all candidates in an event has been studied by comparing the average number of candidates in the δM signal region ($34.8 < \delta M < 41.6 \text{ MeV}/c^2$) and in the lower mass sideband region ($27.8 < \delta M < 34.6 \text{ MeV}/c^2$) in data. To the extent that the average number of candidates is the same in these two regions, there is no bias, as it corresponds to an overall increase in the background level. The average number of candidates in the signal region is 1.0 (1.005) for the signal (sideband) regions for the 1π mode. The corresponding numbers are 1.046 (1.02) for the 3π mode. The difference in the average multiple candidate rate between the signal and sideband regions is assigned as a systematic uncertainty.

The uncertainty in the relative efficiency due to the limited knowledge of the Ξ_b^- lifetime [3] is estimated by weighting the simulated Ξ_b^- decay time to produce a smaller lifetime (1.53 ps) and a larger lifetime (1.61 ps), corresponding to a $\pm 1\sigma$ variation. The relative change in the Ξ_b^- efficiency is assigned as a systematic uncertainty.

6 Results and summary

The two r_s values obtained are averaged, taking the first seven systematic uncertainties in Table 3 as uncorrelated, and the remaining six uncertainties as 100% correlated. The resulting value is

$$\frac{f_{\Xi_b^-}}{f_{\Lambda_b^0}} \mathcal{B}(\Xi_b^- \rightarrow \Lambda_b^0 \pi^-) = (7.3 \pm 0.8 \pm 0.6) \times 10^{-4},$$

where the uncertainties are statistical and total systematic, respectively. Using the independent measurement $\frac{f_{\Xi_b^-}}{f_{\Lambda_b^0}} = (8.2 \pm 0.7 \pm 0.6 \pm 2.5)\%$ [19], the branching fraction is determined to be

$$\mathcal{B}(\Xi_b^- \rightarrow \Lambda_b^0 \pi^-) = (0.89 \pm 0.10 \pm 0.07 \pm 0.29)\%,$$

where the last uncertainty is obtained from the quadrature sum of the uncertainties in $\frac{f_{\Xi_b^-}}{f_{\Lambda_b^0}}$.

The corresponding value obtained from the previous measurements of r_s [18] and $\frac{f_{\Xi_b^-}}{f_{\Lambda_b^0}}$ [19] at 7 and 8 TeV is readily computed to be $\mathcal{B}(\Xi_b^- \rightarrow \Lambda_b^0 \pi^-) = (0.85 \pm 0.27 \pm 0.13 \pm 0.26)\%$. The measurement reported here has about three times better statistical precision.

In summary, using a pp collision data sample at center-of-mass energy 13 TeV collected by the LHCb experiment, corresponding to an integrated luminosity of 5.5 fb^{-1} , the $\Xi_b^- \rightarrow \Lambda_b^0 \pi^-$ decay, in which the b quark is a spectator in the decay process, is observed for the first time. The branching fraction does not show any large enhancements of up to 8% as suggested in Refs. [11, 12]. The measured branching fraction is consistent with the diquark model calculation of 0.69% in Ref. [9], and predictions of (0.19–0.76)% based on current algebra approaches [10, 13, 14], and $(0.63 \pm 0.42)\%$ based on duality [7]. The lower predicted values of $(0.14 \pm 0.07)\%$ using a non-relativistic constituent quark model [8] or 0.2% obtained with the MIT bag model [9] are disfavored. The branching fraction obtained here is also compatible with the naïve ratio of total decay widths of the Λ to Λ_b^0 baryons, which is 0.58%. Although there is no sizeable enhancement in this decay mode, this extra contribution to the Ξ_b^- decay width should be taken into account when comparing the measured Ξ_b^- lifetime to theoretical predictions that only consider the decay of the b quark.

Acknowledgements

We express our gratitude to our colleagues in the CERN accelerator departments for the excellent performance of the LHC. We thank the technical and administrative staff at the LHCb institutes. We acknowledge support from CERN and from the national

agencies: CAPES, CNPq, FAPERJ and FINEP (Brazil); MOST and NSFC (China); CNRS/IN2P3 (France); BMBF, DFG and MPG (Germany); INFN (Italy); NWO (Netherlands); MNiSW and NCN (Poland); MCID/IFA (Romania); MICINN (Spain); SNSF and SER (Switzerland); NASU (Ukraine); STFC (United Kingdom); DOE NP and NSF (USA). We acknowledge the computing resources that are provided by CERN, IN2P3 (France), KIT and DESY (Germany), INFN (Italy), SURF (Netherlands), PIC (Spain), GridPP (United Kingdom), CSCS (Switzerland), IFIN-HH (Romania), CBPF (Brazil), Polish WLCG (Poland) and NERSC (USA). We are indebted to the communities behind the multiple open-source software packages on which we depend. Individual groups or members have received support from ARC and ARDC (Australia); Minciencias (Colombia); AvH Foundation (Germany); EPLANET, Marie Skłodowska-Curie Actions, ERC and NextGenerationEU (European Union); A*MIDEX, ANR, IPhU and Labex P2IO, and Région Auvergne-Rhône-Alpes (France); Key Research Program of Frontier Sciences of CAS, CAS PIFI, CAS CCEPP, Fundamental Research Funds for the Central Universities, and Sci. & Tech. Program of Guangzhou (China); GVA, XuntaGal, GENCAT, Inditex, InTalent and Prog. Atracción Talento, CM (Spain); SRC (Sweden); the Leverhulme Trust, the Royal Society and UKRI (United Kingdom).

References






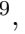





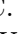


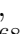

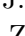




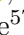
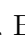

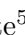


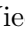



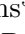
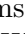
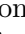

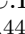
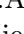
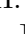

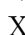



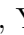

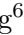

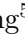
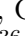
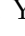




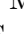
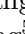



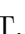
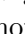





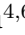

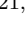





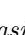


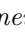
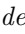


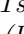
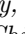


- [1] M. Gell-Mann, *A schematic model of baryons and mesons*, Phys. Lett. **8** (1964) 214.
- [2] G. Zweig, *An SU_3 model for strong interaction symmetry and its breaking; Version 1* CERN-TH-401, CERN, Geneva, 1964.
- [3] Particle Data Group, R. L. Workman *et al.*, *Review of particle physics*, Prog. Theor. Exp. Phys. **2022** (2022) 083C01.
- [4] S. L. Olsen, T. Skwarnicki, and D. Zieminska, *Nonstandard heavy mesons and baryons: Experimental evidence*, Rev. Mod. Phys. **90** (2018) 015003.
- [5] M. Anselmino *et al.*, *Diquarks*, Rev. Mod. Phys. **65** (1993) 1199.
- [6] R. L. Jaffe, *Exotica*, Physics Reports **409** (2005) 1.
- [7] M. Gronau and J. L. Rosner, *S-wave nonleptonic hyperon decays and $\Xi_b^- \rightarrow \pi^- \Lambda_b$* , Phys. Rev. **D93** (2016) 034020.
- [8] P.-Y. Niu, Q. Wang, and Q. Zhao, *Study of heavy quark conserving weak decays in the quark model*, Phys. Lett. **B826** (2022) 136916.
- [9] H.-Y. Cheng *et al.*, *Heavy-flavor-conserving hadronic weak decays of heavy baryons*, JHEP **03** (2016) 028, arXiv:1512.01276.
- [10] S. Faller and T. Mannel, *Light-quark decays in heavy hadrons*, Phys. Lett. **B750** (2015) 653.
- [11] X. Li and M. B. Voloshin, *Decays $\Xi_b \rightarrow \Lambda_b \pi$ and diquark correlations in hyperons*, Phys. Rev. **D90** (2014) 033016, arXiv:1407.2556.
- [12] M. B. Voloshin, *Weak decays $\Xi_Q \rightarrow \Lambda_Q \pi$* , Phys. Lett. **B476** (2000) 297, arXiv:hep-ph/0001057.
- [13] H.-Y. Cheng and F. Xu, *Heavy-flavor-conserving hadronic weak decays of charmed and bottom baryons*, Phys. Rev. **D105** (2022) 094011.
- [14] H.-Y. Cheng, C.-W. Liu, and F. Xu, *Heavy-flavor-conserving hadronic weak decays of charmed and bottom baryons: An update*, Phys. Rev. **D106** (2022) 093005.
- [15] M. Shifman and A. Vainshtein, *Remarks on diquarks, strong binding and a large hidden QCD scale*, Phys. Rev. **D71** (2005) 074010, arXiv:hep-ph/0501200.
- [16] H. G. Dosch, M. Jamin, and B. Stech, *Diquarks, QCD sum rules and weak decays*, Z. Phys. **C42** (1989) 167.
- [17] A. Lenz, *Lifetimes and heavy quark expansion*, Int. J. Mod. Phys. **A30** (2015) 1543005, arXiv:1405.3601.
- [18] LHCb collaboration, R. Aaij *et al.*, *Evidence for the strangeness-changing weak decay $\Xi_b^- \rightarrow \Lambda_b^0 \pi^-$* , Phys. Rev. Lett. **115** (2015) 241801, arXiv:1510.03829.

- [19] LHCb collaboration, R. Aaij *et al.*, *Measurement of the mass and production rate of Ξ_b^- baryons*, Phys. Rev. **D99** (2019) 052006, [arXiv:1901.07075](#).
- [20] LHCb collaboration, R. Aaij *et al.*, *Observation of a new Ξ_b^0 state*, Phys. Rev. **D103** (2021) 012004, [arXiv:2010.14485](#).
- [21] LHCb collaboration, A. A. Alves Jr. *et al.*, *The LHCb detector at the LHC*, JINST **3** (2008) S08005.
- [22] LHCb collaboration, R. Aaij *et al.*, *LHCb detector performance*, Int. J. Mod. Phys. **A30** (2015) 1530022, [arXiv:1412.6352](#).
- [23] R. Aaij *et al.*, *Performance of the LHCb Vertex Locator*, JINST **9** (2014) P09007, [arXiv:1405.7808](#).
- [24] P. d'Argent *et al.*, *Improved performance of the LHCb Outer Tracker in LHC Run 2*, JINST **12** (2017) P11016, [arXiv:1708.00819](#).
- [25] M. Adinolfi *et al.*, *Performance of the LHCb RICH detector at the LHC*, Eur. Phys. J. **C73** (2013) 2431, [arXiv:1211.6759](#).
- [26] A. A. Alves Jr. *et al.*, *Performance of the LHCb muon system*, JINST **8** (2013) P02022, [arXiv:1211.1346](#).
- [27] R. Aaij *et al.*, *Performance of the LHCb trigger and full real-time reconstruction in Run 2 of the LHC*, JINST **14** (2019) P04013, [arXiv:1812.10790](#).
- [28] V. V. Gligorov and M. Williams, *Efficient, reliable and fast high-level triggering using a bonsai boosted decision tree*, JINST **8** (2013) P02013, [arXiv:1210.6861](#).
- [29] T. Likhomanenko *et al.*, *LHCb topological trigger reoptimization*, J. Phys. Conf. Ser. **664** (2015) 082025.
- [30] T. Sjöstrand, S. Mrenna, and P. Skands, *A brief introduction to PYTHIA 8.1*, Comput. Phys. Commun. **178** (2008) 852, [arXiv:0710.3820](#); T. Sjöstrand, S. Mrenna, and P. Skands, *PYTHIA 6.4 physics and manual*, JHEP **05** (2006) 026, [arXiv:hep-ph/0603175](#).
- [31] I. Belyaev *et al.*, *Handling of the generation of primary events in Gauss, the LHCb simulation framework*, J. Phys. Conf. Ser. **331** (2011) 032047.
- [32] D. J. Lange, *The EvtGen particle decay simulation package*, Nucl. Instrum. Meth. **A462** (2001) 152.
- [33] N. Davidson, T. Przedzinski, and Z. Was, *PHOTOS interface in C++: Technical and physics documentation*, Comp. Phys. Comm. **199** (2016) 86, [arXiv:1011.0937](#).
- [34] Geant4 collaboration, J. Allison *et al.*, *Geant4 developments and applications*, IEEE Trans. Nucl. Sci. **53** (2006) 270; Geant4 collaboration, S. Agostinelli *et al.*, *Geant4: A simulation toolkit*, Nucl. Instrum. Meth. **A506** (2003) 250.
- [35] M. Clemencic *et al.*, *The LHCb simulation application, Gauss: Design, evolution and experience*, J. Phys. Conf. Ser. **331** (2011) 032023.

- [36] D. Müller, M. Clemencic, G. Corti, and M. Gersabeck, *ReDecay: A novel approach to speed up the simulation at LHCb*, Eur. Phys. J. **C78** (2018) 1009, [arXiv:1810.10362](#).
- [37] L. Breiman, J. H. Friedman, R. A. Olshen, and C. J. Stone, *Classification and regression trees*, Wadsworth international group, Belmont, California, USA, 1984.
- [38] Y. Freund and R. E. Schapire, *A decision-theoretic generalization of on-line learning and an application to boosting*, J. Comput. Syst. Sci. **55** (1997) 119.
- [39] A. Hoecker *et al.*, *TMVA 4 — Toolkit for Multivariate Data Analysis with ROOT. Users Guide.*, [arXiv:physics/0703039](#).
- [40] M. Pivk and F. R. Le Diberder, *sPlot: A statistical tool to unfold data distributions*, Nucl. Instrum. Meth. **A555** (2005) 356, [arXiv:physics/0402083](#).
- [41] R. Aaij *et al.*, *Selection and processing of calibration samples to measure the particle identification performance of the LHCb experiment in Run 2*, Eur. Phys. J. Tech. Instr. **6** (2019) 1, [arXiv:1803.00824](#).
- [42] T. Skwarnicki, *A study of the radiative cascade transitions between the Upsilon-prime and Upsilon resonances*, PhD thesis, Institute of Nuclear Physics, Krakow, 1986, DESY-F31-86-02.
- [43] LHCb collaboration, R. Aaij *et al.*, *Precision measurement of the mass and lifetime of the Ξ_b^0 baryon*, Phys. Rev. Lett. **113** (2014) 032001, [arXiv:1405.7223](#).
- [44] S. S. Wilks, *The large-sample distribution of the likelihood ratio for testing composite hypotheses*, Ann. Math. Stat. **9** (1938) 60.
- [45] LHCb collaboration, R. Aaij *et al.*, *Measurement of the track reconstruction efficiency at LHCb*, JINST **10** (2015) P02007, [arXiv:1408.1251](#).
- [46] R. Aaij *et al.*, *The LHCb trigger and its performance in 2011*, JINST **8** (2013) P04022, [arXiv:1211.3055](#).

LHCb collaboration

R. Aaij³³, A.S.W. Abdelmotteleb⁵², C. Abellan Beteta⁴⁶, F. Abudinén⁵², T. Ackernley⁵⁶, B. Adeva⁴², M. Adinolfi⁵⁰, P. Adlarson⁷⁸, H. Afsharnia¹⁰, C. Agapopoulou⁴⁴, C.A. Aidala⁷⁹, Z. Ajaltouni¹⁰, S. Akar⁶¹, K. Akiba³³, P. Albicocco²⁴, J. Albrecht¹⁶, F. Alessio⁴⁴, M. Alexander⁵⁵, A. Alfonso Alberro⁴¹, Z. Aliouche⁵⁸, P. Alvarez Cartelle⁵¹, R. Amalric¹⁴, S. Amato², J.L. Amey⁵⁰, Y. Amhis^{12,44}, L. An⁵, L. Anderlini²³, M. Andersson⁴⁶, A. Andreianov³⁹, P. Andreola⁴⁶, M. Andreotti²², D. Andreou⁶⁴, D. Ao⁶, F. Archilli^{32,v}, A. Artamonov³⁹, M. Artuso⁶⁴, E. Aslanides¹¹, M. Atzeni⁶⁰, B. Audurier¹³, D. Bacher⁵⁹, I. Bachiller Perea⁹, S. Bachmann¹⁸, M. Bachmayer⁴⁵, J.J. Back⁵², A. Bailly-reyre¹⁴, P. Baladron Rodriguez⁴², V. Balagura¹³, W. Baldini^{22,44}, J. Baptista de Souza Leite¹, M. Barbeti^{23,m}, I. R. Barbosa⁶⁶, R.J. Barlow⁵⁸, S. Barsuk¹², W. Barter⁵⁴, M. Bartolini⁵¹, F. Baryshnikov³⁹, J.M. Basels¹⁵, G. Bassi^{30,s}, B. Batsukh⁴, A. Battig¹⁶, A. Bay⁴⁵, A. Beck⁵², M. Becker¹⁶, F. Bedeschi³⁰, I.B. Bediaga¹, A. Beiter⁶⁴, S. Belin⁴², V. Bellee⁴⁶, K. Belous³⁹, I. Belov²⁵, I. Belyaev³⁹, G. Benane¹¹, G. Bencivenni²⁴, E. Ben-Haim¹⁴, A. Berezhnoy³⁹, R. Bernet⁴⁶, S. Bernet Andres⁴⁰, D. Berninghoff¹⁸, H.C. Bernstein⁶⁴, C. Bertella⁵⁸, A. Bertolin²⁹, C. Betancourt⁴⁶, F. Betti⁵⁴, J. Bex⁵¹, Ia. Bezshyiko⁴⁶, J. Bhom³⁶, L. Bian⁷⁰, M.S. Bieker¹⁶, N.V. Biesuz²², P. Billoir¹⁴, A. Biolchini³³, M. Birch⁵⁷, F.C.R. Bishop⁵¹, A. Bitadze⁵⁸, A. Bizzeti, M.P. Blago⁵¹, T. Blake⁵², F. Blanc⁴⁵, J.E. Blank¹⁶, S. Blusk⁶⁴, D. Bobulska⁵⁵, V. Bocharnikov³⁹, J.A. Boelhaue¹⁶, O. Boente Garcia¹³, T. Boettcher⁶¹, A. Bohare⁵⁴, A. Boldyrev³⁹, C.S. Bolognani⁷⁶, R. Bolzonella^{22,l}, N. Bondar³⁹, F. Borgato^{29,44}, S. Borghi⁵⁸, M. Borsato¹⁸, J.T. Borsuk³⁶, S.A. Bouchiba⁴⁵, T.J.V. Bowcock⁵⁶, A. Boyer⁴⁴, C. Bozzi²², M.J. Bradley⁵⁷, S. Braun⁶², A. Brea Rodriguez⁴², N. Breer¹⁶, J. Brodzicka³⁶, A. Brossa Gonzalo⁴², J. Brown⁵⁶, D. Brundu²⁸, A. Buonaura⁴⁶, L. Buonincontri²⁹, A.T. Burke⁵⁸, C. Burr⁴⁴, A. Bursche⁶⁸, A. Butkevich³⁹, J.S. Butter³³, J. Buytaert⁴⁴, W. Byczynski⁴⁴, S. Cadeddu²⁸, H. Cai⁷⁰, R. Calabrese^{22,l}, L. Calefice¹⁶, S. Cali²⁴, M. Calvi^{27,p}, M. Calvo Gomez⁴⁰, J. Cambon Bouzas⁴², P. Campana²⁴, D.H. Campora Perez⁷⁶, A.F. Campoverde Quezada⁶, S. Capelli^{27,p}, L. Capriotti²², A. Carbone^{21,j}, L. Carcedo Salgado⁴², R. Cardinale^{25,n}, A. Cardini²⁸, P. Carniti^{27,p}, L. Carus¹⁸, A. Casais Vidal⁴², R. Caspary¹⁸, G. Casse⁵⁶, M. Cattaneo⁴⁴, G. Cavallero²², V. Cavallini^{22,l}, S. Celani⁴⁵, J. Cerasoli¹¹, D. Cervenkov⁵⁹, A.J. Chadwick⁵⁶, I. Chahrouh⁷⁹, M.G. Chapman⁵⁰, M. Charles¹⁴, Ph. Charpentier⁴⁴, C.A. Chavez Barajas⁵⁶, M. Chefdeville⁹, C. Chen¹¹, S. Chen⁴, A. Chernov³⁶, S. Chernyshenko⁴⁸, V. Chobanova^{42,y}, S. Cholak⁴⁵, M. Chrzaszcz³⁶, A. Chubykin³⁹, V. Chulikov³⁹, P. Ciambone²⁴, M.F. Cicala⁵², X. Cid Vidal⁴², G. Ciezarek⁴⁴, P. Cifra⁴⁴, G. Ciullo^{l,22}, P.E.L. Clarke⁵⁴, M. Clemencic⁴⁴, H.V. Cliff⁵¹, J. Closier⁴⁴, J.L. Cobbledick⁵⁸, C. Cocha Toapaxi¹⁸, V. Coco⁴⁴, J. Cogan¹¹, E. Cogneras¹⁰, L. Cojocariu³⁸, P. Collins⁴⁴, T. Colombo⁴⁴, A. Comerma-Montells⁴¹, L. Congedo²⁰, A. Contu²⁸, N. Cooke⁵⁵, I. Corredoira⁴², A. Correia¹⁴, G. Corti⁴⁴, J.J. Cottee Meldrum⁵⁰, B. Couturier⁴⁴, D.C. Craik⁴⁶, M. Cruz Torres^{1,h}, R. Currie⁵⁴, C.L. Da Silva⁶³, S. Dadabaev³⁹, L. Dai⁶⁷, X. Dai⁵, E. Dall’Occo¹⁶, J. Dalseno⁴², C. D’Ambrosio⁴⁴, J. Daniel¹⁰, A. Danilina³⁹, P. d’Argent²⁰, A. Davidson⁵², J.E. Davies⁵⁸, A. Davis⁵⁸, O. De Aguiar Francisco⁵⁸, J. de Boer³³, K. De Bruyn⁷⁵, S. De Capua⁵⁸, M. De Cian¹⁸, U. De Freitas Carneiro Da Graca^{1,b}, E. De Lucia²⁴, J.M. De Miranda¹, L. De Paula², M. De Serio^{20,i}, D. De Simone⁴⁶, P. De Simone²⁴, F. De Vellis¹⁶, J.A. de Vries⁷⁶, C.T. Dean⁶³, F. Debernardis^{20,i}, D. Decamp⁹,

X. Vilasis-Cardona⁴⁰ , E. Vilella Figueras⁵⁶ , A. Villa²¹ , P. Vincent¹⁴ , F.C. Volle¹² , D. vom Bruch¹¹ , V. Vorobyev³⁹ , N. Voropaev³⁹ , K. Vos⁷⁶ , C. Vrahas⁵⁴ , J. Walsh³⁰ , E.J. Walton⁶⁵ , G. Wan⁵ , C. Wang¹⁸ , G. Wang⁷ , J. Wang⁵ , J. Wang⁴ , J. Wang³ , J. Wang⁷⁰ , M. Wang²⁶ , N. W. Wang⁶ , R. Wang⁵⁰ , X. Wang⁶⁸ , Y. Wang⁷ , Z. Wang⁴⁶ , Z. Wang³ , Z. Wang⁶ , J.A. Ward^{52,65} , N.K. Watson⁴⁹ , D. Websdale⁵⁷ , Y. Wei⁵ , B.D.C. Westhenry⁵⁰ , D.J. White⁵⁸ , M. Whitehead⁵⁵ , A.R. Wiederhold⁵² , D. Wiedner¹⁶ , G. Wilkinson⁵⁹ , M.K. Wilkinson⁶¹ , I. Williams⁵¹ , M. Williams⁶⁰ , M.R.J. Williams⁵⁴ , R. Williams⁵¹ , F.F. Wilson⁵³ , W. Wislicki³⁷ , M. Witek³⁶ , L. Witola¹⁸ , C.P. Wong⁶³ , G. Wormser¹² , S.A. Wotton⁵¹ , H. Wu⁶⁴ , J. Wu⁷ , Y. Wu⁵ , K. Wyllie⁴⁴ , S. Xian⁶⁸ , Z. Xiang⁴ , Y. Xie⁷ , A. Xu³⁰ , J. Xu⁶ , L. Xu³ , L. Xu³ , M. Xu⁵² , Z. Xu¹⁰ , Z. Xu⁶ , Z. Xu⁴ , D. Yang³ , S. Yang⁶ , X. Yang⁵ , Y. Yang²⁵ , Z. Yang⁵ , Z. Yang⁶² , V. Yeroshenko¹² , H. Yeung⁵⁸ , H. Yin⁷ , C. Y. Yu⁵ , J. Yu⁶⁷ , X. Yuan⁴ , E. Zaffaroni⁴⁵ , M. Zavertyaev¹⁷ , M. Zdybal³⁶ , M. Zeng³ , C. Zhang⁵ , D. Zhang⁷ , J. Zhang⁶ , L. Zhang³ , S. Zhang⁶⁷ , S. Zhang⁵ , Y. Zhang⁵ , Y. Zhang⁵⁹ , Y. Zhao¹⁸ , A. Zharkova³⁹ , A. Zhelezov¹⁸ , Y. Zheng⁶ , T. Zhou⁵ , X. Zhou⁷ , Y. Zhou⁶ , V. Zhovkovska¹² , L. Z. Zhu⁶ , X. Zhu³ , X. Zhu⁷ , Z. Zhu⁶ , V. Zhukov^{15,39} , J. Zhuo⁴³ , Q. Zou^{4,6} , S. Zucchelli^{21,j} , D. Zuliani²⁹ , G. Zunica⁵⁸ .

¹ Centro Brasileiro de Pesquisas Físicas (CBPF), Rio de Janeiro, Brazil

² Universidade Federal do Rio de Janeiro (UFRJ), Rio de Janeiro, Brazil

³ Center for High Energy Physics, Tsinghua University, Beijing, China

⁴ Institute Of High Energy Physics (IHEP), Beijing, China

⁵ School of Physics State Key Laboratory of Nuclear Physics and Technology, Peking University, Beijing, China

⁶ University of Chinese Academy of Sciences, Beijing, China

⁷ Institute of Particle Physics, Central China Normal University, Wuhan, Hubei, China

⁸ Consejo Nacional de Rectores (CONARE), San Jose, Costa Rica

⁹ Université Savoie Mont Blanc, CNRS, IN2P3-LAPP, Annecy, France

¹⁰ Université Clermont Auvergne, CNRS/IN2P3, LPC, Clermont-Ferrand, France

¹¹ Aix Marseille Univ, CNRS/IN2P3, CPPM, Marseille, France

¹² Université Paris-Saclay, CNRS/IN2P3, IJCLab, Orsay, France

¹³ Laboratoire Leprince-Ringuet, CNRS/IN2P3, Ecole Polytechnique, Institut Polytechnique de Paris, Palaiseau, France

¹⁴ LPNHE, Sorbonne Université, Paris Diderot Sorbonne Paris Cité, CNRS/IN2P3, Paris, France

¹⁵ I. Physikalisches Institut, RWTH Aachen University, Aachen, Germany

¹⁶ Fakultät Physik, Technische Universität Dortmund, Dortmund, Germany

¹⁷ Max-Planck-Institut für Kernphysik (MPIK), Heidelberg, Germany

¹⁸ Physikalisches Institut, Ruprecht-Karls-Universität Heidelberg, Heidelberg, Germany

¹⁹ School of Physics, University College Dublin, Dublin, Ireland

²⁰ INFN Sezione di Bari, Bari, Italy

²¹ INFN Sezione di Bologna, Bologna, Italy

²² INFN Sezione di Ferrara, Ferrara, Italy

²³ INFN Sezione di Firenze, Firenze, Italy

²⁴ INFN Laboratori Nazionali di Frascati, Frascati, Italy

²⁵ INFN Sezione di Genova, Genova, Italy

²⁶ INFN Sezione di Milano, Milano, Italy

²⁷ INFN Sezione di Milano-Bicocca, Milano, Italy

²⁸ INFN Sezione di Cagliari, Monserrato, Italy

²⁹ Università degli Studi di Padova, Università e INFN, Padova, Padova, Italy

³⁰ INFN Sezione di Pisa, Pisa, Italy

³¹ INFN Sezione di Roma La Sapienza, Roma, Italy

³² INFN Sezione di Roma Tor Vergata, Roma, Italy

³³ Nikhef National Institute for Subatomic Physics, Amsterdam, Netherlands

- ³⁴ *Nikhef National Institute for Subatomic Physics and VU University Amsterdam, Amsterdam, Netherlands*
- ³⁵ *AGH - University of Science and Technology, Faculty of Physics and Applied Computer Science, Kraków, Poland*
- ³⁶ *Henryk Niewodniczanski Institute of Nuclear Physics Polish Academy of Sciences, Kraków, Poland*
- ³⁷ *National Center for Nuclear Research (NCBJ), Warsaw, Poland*
- ³⁸ *Horia Hulubei National Institute of Physics and Nuclear Engineering, Bucharest-Magurele, Romania*
- ³⁹ *Affiliated with an institute covered by a cooperation agreement with CERN*
- ⁴⁰ *DS4DS, La Salle, Universitat Ramon Llull, Barcelona, Spain*
- ⁴¹ *ICCUB, Universitat de Barcelona, Barcelona, Spain*
- ⁴² *Instituto Galego de Física de Altas Enerxías (IGFAE), Universidade de Santiago de Compostela, Santiago de Compostela, Spain*
- ⁴³ *Instituto de Física Corpuscular, Centro Mixto Universidad de Valencia - CSIC, Valencia, Spain*
- ⁴⁴ *European Organization for Nuclear Research (CERN), Geneva, Switzerland*
- ⁴⁵ *Institute of Physics, Ecole Polytechnique Fédérale de Lausanne (EPFL), Lausanne, Switzerland*
- ⁴⁶ *Physik-Institut, Universität Zürich, Zürich, Switzerland*
- ⁴⁷ *NSC Kharkiv Institute of Physics and Technology (NSC KIPT), Kharkiv, Ukraine*
- ⁴⁸ *Institute for Nuclear Research of the National Academy of Sciences (KINR), Kyiv, Ukraine*
- ⁴⁹ *University of Birmingham, Birmingham, United Kingdom*
- ⁵⁰ *H.H. Wills Physics Laboratory, University of Bristol, Bristol, United Kingdom*
- ⁵¹ *Cavendish Laboratory, University of Cambridge, Cambridge, United Kingdom*
- ⁵² *Department of Physics, University of Warwick, Coventry, United Kingdom*
- ⁵³ *STFC Rutherford Appleton Laboratory, Didcot, United Kingdom*
- ⁵⁴ *School of Physics and Astronomy, University of Edinburgh, Edinburgh, United Kingdom*
- ⁵⁵ *School of Physics and Astronomy, University of Glasgow, Glasgow, United Kingdom*
- ⁵⁶ *Oliver Lodge Laboratory, University of Liverpool, Liverpool, United Kingdom*
- ⁵⁷ *Imperial College London, London, United Kingdom*
- ⁵⁸ *Department of Physics and Astronomy, University of Manchester, Manchester, United Kingdom*
- ⁵⁹ *Department of Physics, University of Oxford, Oxford, United Kingdom*
- ⁶⁰ *Massachusetts Institute of Technology, Cambridge, MA, United States*
- ⁶¹ *University of Cincinnati, Cincinnati, OH, United States*
- ⁶² *University of Maryland, College Park, MD, United States*
- ⁶³ *Los Alamos National Laboratory (LANL), Los Alamos, NM, United States*
- ⁶⁴ *Syracuse University, Syracuse, NY, United States*
- ⁶⁵ *School of Physics and Astronomy, Monash University, Melbourne, Australia, associated to ⁵²*
- ⁶⁶ *Pontifícia Universidade Católica do Rio de Janeiro (PUC-Rio), Rio de Janeiro, Brazil, associated to ²*
- ⁶⁷ *Physics and Micro Electronic College, Hunan University, Changsha City, China, associated to ⁷*
- ⁶⁸ *Guangdong Provincial Key Laboratory of Nuclear Science, Guangdong-Hong Kong Joint Laboratory of Quantum Matter, Institute of Quantum Matter, South China Normal University, Guangzhou, China, associated to ³*
- ⁶⁹ *Lanzhou University, Lanzhou, China, associated to ⁴*
- ⁷⁰ *School of Physics and Technology, Wuhan University, Wuhan, China, associated to ³*
- ⁷¹ *Departamento de Física, Universidad Nacional de Colombia, Bogota, Colombia, associated to ¹⁴*
- ⁷² *Universität Bonn - Helmholtz-Institut für Strahlen und Kernphysik, Bonn, Germany, associated to ¹⁸*
- ⁷³ *Eotvos Lorand University, Budapest, Hungary, associated to ⁴⁴*
- ⁷⁴ *INFN Sezione di Perugia, Perugia, Italy, associated to ²²*
- ⁷⁵ *Van Swinderen Institute, University of Groningen, Groningen, Netherlands, associated to ³³*
- ⁷⁶ *Universiteit Maastricht, Maastricht, Netherlands, associated to ³³*
- ⁷⁷ *Tadeusz Kosciuszko Cracow University of Technology, Cracow, Poland, associated to ³⁶*
- ⁷⁸ *Department of Physics and Astronomy, Uppsala University, Uppsala, Sweden, associated to ⁵⁵*
- ⁷⁹ *University of Michigan, Ann Arbor, MI, United States, associated to ⁶⁴*
- ⁸⁰ *Departement de Physique Nucleaire (SPhN), Gif-Sur-Yvette, France*

^a *Universidade de Brasília, Brasília, Brazil*

^b *Centro Federal de Educação Tecnológica Celso Suckow da Fonseca, Rio De Janeiro, Brazil*

^c *Universidade Federal do Triângulo Mineiro (UFTM), Uberaba-MG, Brazil*

^d *Central South U., Changsha, China*

- ^e Hangzhou Institute for Advanced Study, UCAS, Hangzhou, China
^f LIP6, Sorbonne Universite, Paris, France
^g Excellence Cluster ORIGINS, Munich, Germany
^h Universidad Nacional Autónoma de Honduras, Tegucigalpa, Honduras
ⁱ Università di Bari, Bari, Italy
^j Università di Bologna, Bologna, Italy
^k Università di Cagliari, Cagliari, Italy
^l Università di Ferrara, Ferrara, Italy
^m Università di Firenze, Firenze, Italy
ⁿ Università di Genova, Genova, Italy
^o Università degli Studi di Milano, Milano, Italy
^p Università di Milano Bicocca, Milano, Italy
^q Università di Padova, Padova, Italy
^r Università di Perugia, Perugia, Italy
^s Scuola Normale Superiore, Pisa, Italy
^t Università di Pisa, Pisa, Italy
^u Università della Basilicata, Potenza, Italy
^v Università di Roma Tor Vergata, Roma, Italy
^w Università di Urbino, Urbino, Italy
^x Universidad de Alcalá, Alcalá de Henares, Spain
^y Universidade da Coruña, Coruña, Spain
[†] Deceased